Earth and Planetary Science Letters 498 (2018) 309–321

Contents lists available at ScienceDirect

Earth and Planetary Science Letters

www.elsevier.com/locate/epsl

Plate tectonic cycling modulates Earth's $^{3}He/^{22}Ne$ ratio

Nick Dygert [a,b,*], Colin R.M. Jackson [c,d], Marc A. Hesse [a], Marissa M. Tremblay [e,f,g], David L. Shuster [e,f], Jesse T. Gu [a]

[a] Department of Geological Sciences, Jackson School of Geosciences, University of Texas at Austin, Austin, TX 78712, United States of America
[b] Planetary Geosciences Institute, Department of Earth and Planetary Sciences, University of Tennessee, Knoxville, Knoxville, TN 37996, United States of America
[c] Geophysical Laboratory, Carnegie Institution for Science, Washington, DC 20015, United States of America
[d] National Museum of Natural History, Smithsonian Institution, Washington, DC 20560, United States of America
[e] Department of Earth and Planetary Science, University of California, Berkeley, Berkeley, CA 94720, United States of America
[f] Berkeley Geochronology Center, Berkeley, CA 94709, United States of America
[g] Scottish Universities Environmental Research Centre, East Kilbride, Scotland G75 0QF, UK

ARTICLE INFO

Article history:
Received 10 January 2018
Received in revised form 16 May 2018
Accepted 27 June 2018
Available online 20 July 2018
Editor: M. Bickle

Keywords:
$^{3}He/^{22}Ne$
noble gas
dunite channel
kinetic fractionation
diffusion
mantle lithosphere

ABSTRACT

The ratio of ^{3}He and ^{22}Ne varies throughout the mantle. This observation is surprising because ^{3}He and ^{22}Ne are not produced in the mantle, are highly incompatible during mantle melting, and are not recycled back into the mantle by subduction of oceanic sediment or basaltic crust. Our new compilation yields average $^{3}He/^{22}Ne$ ratios of 7.5 ± 1.2 and 3.5 ± 2.4 for mid-ocean ridge basalt (MORB) mantle and ocean island basalt (OIB) mantle sources respectively. The low $^{3}He/^{22}Ne$ of OIB mantle approaches planetary precursor $^{3}He/^{22}Ne$ values; ~1 for chondrites and ~1.5 for the solar nebula. The high $^{3}He/^{22}Ne$ of the MORB mantle is not similar to any planetary precursor, requiring a mechanism for fractionating He from Ne in the mantle and suggesting isolation of distinct mantle reservoirs throughout geologic time. New experimental results reported here demonstrate that He and Ne diffuse at rates differing by one or more orders of magnitude at relevant temperatures in mantle materials. We model the formation of a MORB mantle with an elevated $^{3}He/^{22}Ne$ ratio through kinetically modulated chemical exchange between dunite channel-hosted basaltic liquids and harzburgite wallrock beneath mid-ocean ridges. Over timescales relevant to mantle upwelling beneath spreading centers, He may diffuse tens to hundreds of meters into wallrock while Ne is effectively immobile, producing a mantle lithosphere regassed with respect to He and depleted with respect to Ne, with a net elevated $^{3}He/^{22}Ne$. Subduction of high $^{3}He/^{22}Ne$ mantle lithosphere throughout geologic time would generate a MORB source with high $^{3}He/^{22}Ne$. Mixing models suggest that to preserve a high $^{3}He/^{22}Ne$ reservoir, MORB mantle mixing timescales must be on the order of hundreds of millions of years or longer, that mantle convection has not been layered about the transition zone for most of geologic time, and that Earth's convecting mantle has lost at least 96% of its primordial volatile elements. The most depleted, highest $^{3}He/^{22}Ne$ mantle may be best preserved in the lower mantle where relatively high viscosities impede mechanical mixing.

1. Introduction

^{3}He and ^{22}Ne are not produced in the mantle or fractionated by partial melting, and neither isotope is recycled back into the mantle by subduction of oceanic basalt or sediment (e.g., Heber et al., 2007; Hilton et al., 2002; Jackson et al., 2013a; Staudacher and Allègre, 1988; Tucker and Mukhopadhyay, 2014). Thus, it is a surprise that large $^{3}He/^{22}Ne$ variations exist within mantle-derived rocks and that by inference; the mantle has a net elevated $^{3}He/^{22}Ne$ ratio compared to volatile-rich planetary precursor materials such as the solar nebula, chondritic meteorites, iron meteorites and achondrites (Fig. 1, Graham, 2002; Harper and Jacobsen, 1996; Honda and McDougall, 1998; Ott, 2002). $^{3}He/^{22}Ne$ ratios may preserve a unique record of mantle evolution, provided mechanisms for fractionating He from Ne in the mantle are understood.

Previous work (Graham, 2002; Honda and McDougall, 1998) and the updated compilation presented in this manuscript (Fig. 1; Supplementary Table 1) show that the mid-ocean ridge basalt (MORB) mantle source has distinctly higher $^{3}He/^{22}Ne$ compared to ocean island basalt (OIB) sources (7.5 ± 1.2 and 3.5 ± 2.4 respectively; see the electronic supplement for a description of our

* Corresponding author at: Department of Earth and Planetary Sciences, University of Tennessee, Knoxville, 1621 Cumberland Avenue, 602 Strong Hall, Knoxville, TN 37996, United States of America.
E-mail address: ndygert1@utk.edu (N. Dygert).

https://doi.org/10.1016/j.epsl.2018.06.044
0012-821X/

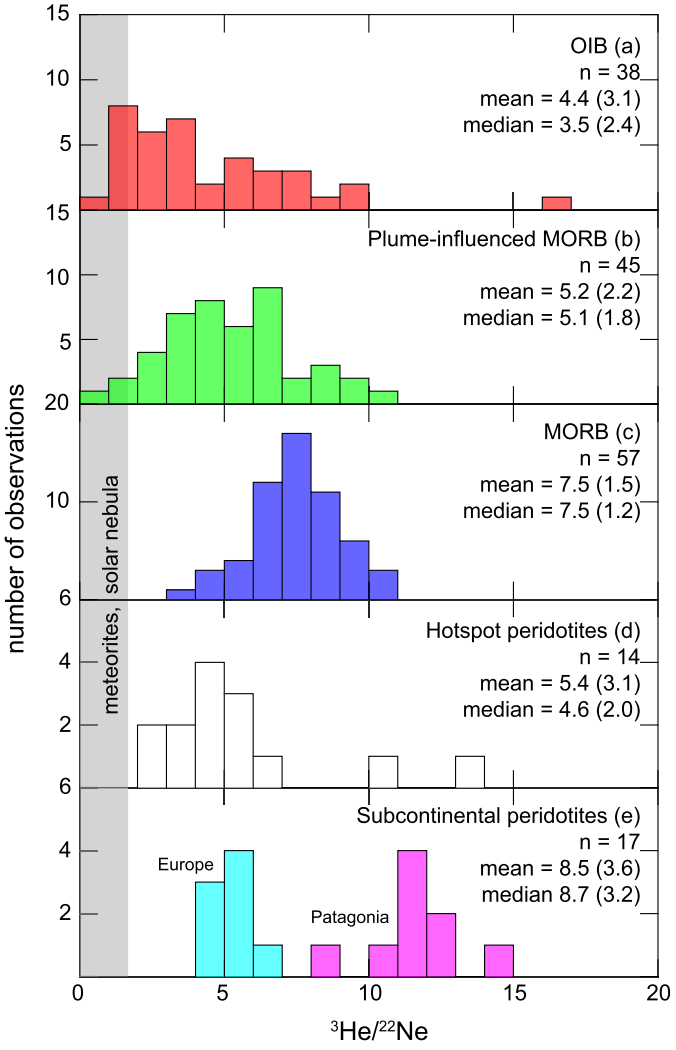

Fig. 1. $^3He/^{22}Ne$ ratios of ocean island basalts (a), plume-influenced MORBs (b), MORBs (c), hotspot sourced mantle xenoliths (d), and subcontinental lithospheric mantle (e). $^3He/^{22}Ne$ for all samples are calculated using methods detailed in the electronic supplement. Data used to calculate ratios for subaerial samples are exclusively from crush steps in order to minimize any contribution from a cosmogenic component. Shown in parentheses are the standard deviation (mean) and median absolute deviation (median). Data source references are presented in the Electronic Supplement; the compilation is downloadable from the electronic repository. Sample localities are the following; OIBs: Galapagos, Samoa, Iceland, Reunion, Hawaii; plume-influenced MORBs: Azores, Discovery, Shona, East Pacific Rise, Galapagos Ridge, Southeast Indian Ridge; MORBs: Mid Atlantic Ridge; East Pacific Rise; Chile Ridge, Southwest Indian Ridge; hotspot sourced xenoliths: Hawaii, Mt. Cameroon, Kerguelen, Biu Plateau, Reunion, Samoa; subcontinental lithospheric peridotites: Szentbekalla (Hungary), Dreiser Weiher (Germany), Laguna Ana; Laguna Timone; Governador Gregores (Patagonia). In all cases, we deferred to the interpretations of our data sources to assign a sample type, which were assigned based on $^3He/^4He$ and radiogenic isotope ratios.

methods). The low $^3He/^{22}Ne$ of OIBs approaches chondritic (∼1) and solar nebula values (∼1.5), whereas the high $^3He/^{22}Ne$ of the MORB mantle is not similar to solar sources or any known family of meteorites. Such a high $^3He/^{22}Ne$ ratio for MORB mantle requires a mechanism for fractionating He from Ne in the mantle and suggests isolation of distinct mantle reservoirs during Earth's evolution.

The current model for forming a mantle heterogeneous in $^3He/^{22}Ne$ invokes fractionation from magma ocean degassing (Honda and McDougall, 1998; Tucker and Mukhopadhyay, 2014). He is ∼2× more soluble than Ne in peridotitic melt (e.g., Iacono-Marziano et al., 2010); degassing a magma ocean to form a primitive atmosphere would elevate the $^3He/^{22}Ne$ of the magma ocean. In a best-case scenario under equilibrium conditions, a degassing event roughly doubles the $^3He/^{22}Ne$ of the magma ocean. Subsequent degassing events can only further fractionate mantle $^3He/^{22}Ne$ ratios if there is atmospheric blow-off prior to the next period of magma ocean–atmosphere equilibration.

Primordial sources of He and Ne have $^3He/^{22}Ne$ ratios of ∼1.5 (e.g., Harper and Jacobsen, 1996; Mahaffy et al., 1998; Ott, 2002; Trieloff and Kunz, 2005). Thus, accounting for $^3He/^{22}Ne$ ratios above 10 (e.g., Fig. 1, Graham, 2002; Honda and McDougall, 1998; Tucker and Mukhopadhyay, 2014) requires >2 magma ocean degassing events affecting the MORB mantle, and complete atmospheric blow-off prior to each magma ocean event. If He is rapidly lost from the atmosphere, as is the case today, between magma oceans, subsequent atmosphere–magma ocean equilibration would lead to a decreased $^3He/^{22}Ne$ ratio in the mantle, rather than the proposed increase.

Here we explore the possibility that elevated $^3He/^{22}Ne$ ratios relate to diffusion kinetics of He and Ne. It has long been known that He, Ne, and heavier noble gases have high-temperature diffusivities that differ by orders of magnitude in igneous materials (e.g., Behrens, 2010; Baxter, 2010 and references therein), providing the potential for kinetic fractionation of He from Ne in the mantle. The importance of kinetic fractionation for producing isotopic and trace element variations has been investigated previously (e.g., Albarède, 2008; Barfod et al., 1999; Dygert et al., 2016; Hart, 1993; Hofmann and Hart, 1978; Kenyon, 1990, 1993; Spiegelman and Kenyon, 1992). Kinetic fractionation has been invoked to explain noble gas systematics in basalts that may be consistent with disequilibrium melting (e.g., Burnard, 2004; Burnard et al., 2004; Yamamoto et al., 2009). Here, instead of focusing on mantle melts, we evaluate how differences in He and Ne diffusivities can affect the compositions of mantle melting residues. We model the formation of an elevated and variable $^3He/^{22}Ne$ MORB source through kinetically modulated chemical exchange between dunite channel-hosted basaltic liquids and harzburgite wallrock beneath mid-ocean ridges. We demonstrate that kinetic fractionation of He and Ne will occur as basaltic liquids migrate through upwelling mantle, a process known to occur within Earth for billions of years. Our model predicts observed correlations between $^3He/^{22}Ne$ ratios and indices of depletion, including La/Sm, and the Rb–Sr and Sm–Nd isotope systems. It requires the entire high $^3He/^{22}Ne$ source to have fluxed through the global mid-ocean ridge system at least once, effective mantle mixing timescales of 0.4 Gyr or longer, and suggests that convection of the MORB mantle across the transition zone has dominated throughout geologic time.

1.1. Melt transport in dunite channels

Tabular bodies of olivine (dunites) are observed in ophiolites and interpreted to form a tree-root like network of high-porosity pathways called dunite channels. Dunite channel networks are thought to efficiently focus and extract mantle melts produced by adiabatic decompression melting beneath mid-ocean ridges (Fig. 2; Kelemen et al., 1995, 1997). Channelization necessarily juxtaposes dunite-hosted basaltic melts against harzburgitic melting residues (e.g., Liang et al., 2010; Schiemenz et al., 2010; Spiegelman et al., 2001; Spiegelman and Kelemen, 2003). Field observations demonstrate that dunite-hosted basaltic melts and adjacent harzburgite wallrock are not in chemical equilibrium (e.g., Dygert et al., 2016; Kelemen et al., 1992, 1995; Suhr et al., 2003), which inevitably leads to some amount of diffusive exchange (e.g., Burnard, 2004; Burnard et al., 2004; Kenyon, 1990, 1993; Spiegelman and Kenyon, 1992). The extent of diffusive interaction between the dunite-hosted basaltic melt and adjacent wallrock depends on the effective diffusion rate of the element in the wallrock.

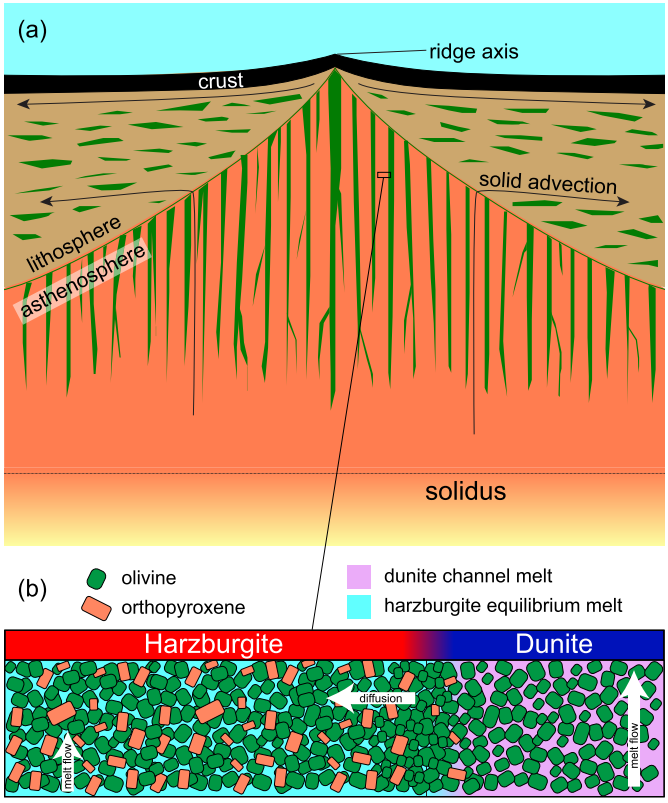

Fig. 2. Schematic of a dunite channel network in a triangular melting region beneath a mid-ocean ridge (a). Arrows show paths of solid advection. Partial melts are focused and extracted in tabular dunite bodies (green). (b) Close-up showing dunite–wallrock relationships. Between the dunite and harzburgite wallrock is a compacting boundary layer with a low melt fraction. Note the harzburgite wallrock and dunite channel host melts with distinct compositions, in local equilibrium with their host matrix. (For interpretation of the colors in the figure(s), the reader is referred to the web version of this article.)

2. He and Ne diffusion rates in mantle materials

2.1. Measurements

Helium is significantly lighter and smaller than Ne and is therefore expected to diffuse faster than Ne in silicate melts and minerals at mantle temperatures. Relatively high He diffusivity would lead to kinetic fractionation of He from Ne (and heavier noble gases) in harzburgite wallrock around dunite channels. Despite the clear expectation for faster He diffusion than Ne, reported Arrhenius relationships for He and Ne are highly scattered. Measurements of Ne and He diffusion rates in mantle-relevant materials are summarized in Fig. 3; lattice diffusion in olivine is shown in Fig. 3a, diffusion in silicate glasses is shown in Fig. 3b, grain boundary diffusion is shown in Fig. 3c. These studies comprise a variety of experimental approaches including first-principles calculations (Wang et al., 2015), high-pressure gas-soaking (Cherniak et al., 2014) and implantation degassing experiments (Cherniak and Watson, 2012; Cherniak et al., 2014), bulk degassing of natural and proton irradiated materials (Blard et al., 2008; Burnard et al., 2015; Futagami et al., 1993; Gourbet et al., 2012; Shuster et al., 2004; Tolstikhin et al., 2010; this study), and glass membrane (Frank et al., 1961; Swets et al., 1961), bubble shrinkage (Frischat and Oel, 1965; Wendler et al., 1995), and desorption experiments (Mulfinger and Scholze, 1962). An unrepeated preliminary experiment conducted at a single temperature on a superliquidus basaltic melt suggests $D_{He} > D_{Ne}$ (Lux, 1987). A recent study on CMAS glass and superliquidus melt found $D_{He} > D_{Ar}$ at a temperature of 1300 °C, but a He diffusion rate significantly slower than previous work (Amalberti et al., 2018). Here we adopt an assumption common to the noble gas literature (e.g. Gonnermann and Mukhopadhyay, 2007; Weston et al., 2015), that Arrhenius relations for He and Ne diffusion rates in simple silicate glasses can be extrapolated to mantle temperatures to approximate high-temperature diffusion in basaltic melts (green squares, Fig. 3d).

Data summarized in Fig. 3 collectively suggest that while measured diffusion rates vary among references for a particular element, Ne diffuses one or more orders of magnitude more slowly than He in mantle minerals and melts at mantle-relevant temperatures (Fig. 3d). A notable exception is the study of Gourbet et al., 2012 (green line, Fig. 3a), which measured bulk diffusion of Ne in proton-irradiated olivine using a step-heating technique. Gourbet et al. (2012) observed Ne diffusion rates orders of magnitude faster than other work (Cherniak et al., 2014; Futagami et al., 1993), and found that Ne and He diffuse at similar rates at high temperature.

To evaluate the discrepancy among measurements of Ne diffusion in olivine, we conducted a new bulk degassing experiment on a single crystal fragment from the batch of proton-irradiated San Carlos olivine previously investigated by Gourbet et al. (2012). We selected a grain with relatively few inclusions and cracks (Supplementary Fig. S1), in contrast to grains investigated by Gourbet et al. (2012) (see their Supplementary Fig. S2a). ^{3}He and ^{21}Ne were analyzed simultaneously during degassing, allowing us to directly compare their diffusivities throughout the experiment. Bulk degassing data were interpreted assuming a spherical geometry using equations presented in Fechtig and Kalbitzer (1966). Results are shown in Fig. 4 and Supplementary Fig. S2; experimental, analytical and interpretive methods are discussed in detail in the Electronic Supplement. Except for some final He steps (collected after >99% degassing and barely above the instrumental detection limit, unfilled red circles, Fig. 4), all data collected while temperatures were well resolved are included in our analysis for both He and Ne.

The experiment yields activation energies of 122.1 ± 5.1 kJ/mol for He and 168.6 ± 8.8 kJ/mol for Ne. An effective spherical olivine radius of 330 μm gives Arrhenius preexponentials of $8.80 \times 10^{-7}{}^{+7.89\times10^{-7}}_{-4.16\times10^{-7}}$ for He and $1.25 \times 10^{-6}{}^{+1.70\times10^{-6}}_{-7.21\times10^{-7}}$ for Ne. In that He diffuses significantly faster than Ne at all experimental temperatures, our results are consistent with the work of Futagami et al. (1993) and Cherniak et al. (2014). However, we observe high-temperature Ne diffusion rates orders of magnitude more rapid than either of these previous studies (compare thick blue and magenta lines, Fig. 3a). The cause of the discrepancy is unknown, but it could be related to differences in analytical and/or experimental methods, data interpretation, or the presence of optically unobservable diffusive fast paths or multiple diffusion domains in the relatively large olivine crystal fragment we analyzed (e.g., cracks, cf. Cherniak et al., 2014). The latter is not supported by our He data, which agree well with diffusivities given by other recent studies (Fig. 3a; Blard et al., 2008; Cherniak and Watson, 2012; Shuster et al., 2004; Tolstikhin et al., 2010; Wang et al., 2015). We note that unlike prior work, our Ne activation energy is greater than that of He, consistent with diffusion compensation theory (e.g., Hofmann, 1980; Winchell, 1969).

2.2. Pathways for diffusive exchange between dunite channels and wallrock

To model kinetic fractionation of He from Ne around dunite channels, we must consider which diffusive mechanisms produce the largest flux of noble gases into harzburgite wallrock. Diffusion of Ne along grain boundaries has not been measured, but recent work suggests He and Ar diffusion along olivine grain boundaries is slower than olivine lattice diffusion when grain boundary Arrhenius relations are extrapolated to mantle temperatures (Fig. 3c;

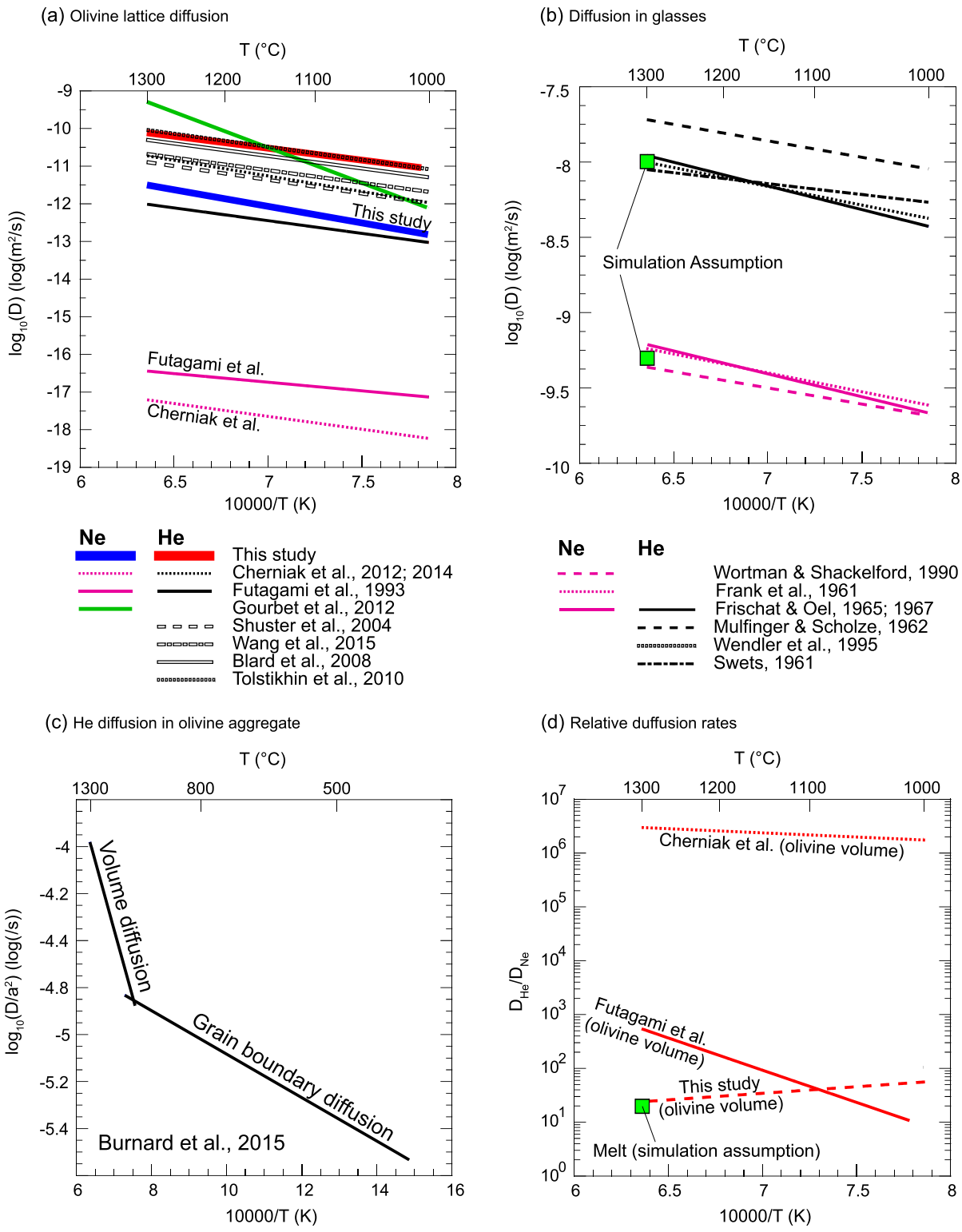

Fig. 3. Measured rates of He and Ne diffusion in the olivine lattice (a) and silicate glasses (b); He diffusion along olivine aggregate grain boundaries (c); and relative diffusion rates of He and Ne as a function of temperature (d) for experiments from three laboratories. Glass data are extrapolated from lower temperature experimental observations through the glass–liquid transition, and are from simple compositional systems which may differ structurally from basaltic glasses.

Burnard et al., 2015; Delon et al., 2018). We assume Ne behaves similarly.

Diffusion through a network of interconnected melt at the dunite channel–wallrock interface would facilitate diffusive exchange, as noble gas diffusion in melts is assumed to be $\gtrsim$2 orders of magnitude faster than in the olivine lattice (compare Figs. 3b and 3a), and noble gases are highly soluble in melts relative to minerals (e.g., Heber et al., 2007; Jackson et al., 2013a). However, numerical simulations suggest the melt fraction around dunite channels may be at or below the "permeability threshold", i.e., the minimum melt fraction needed to produce an interconnected melt network (if such a threshold exists). Melt suction into the lower

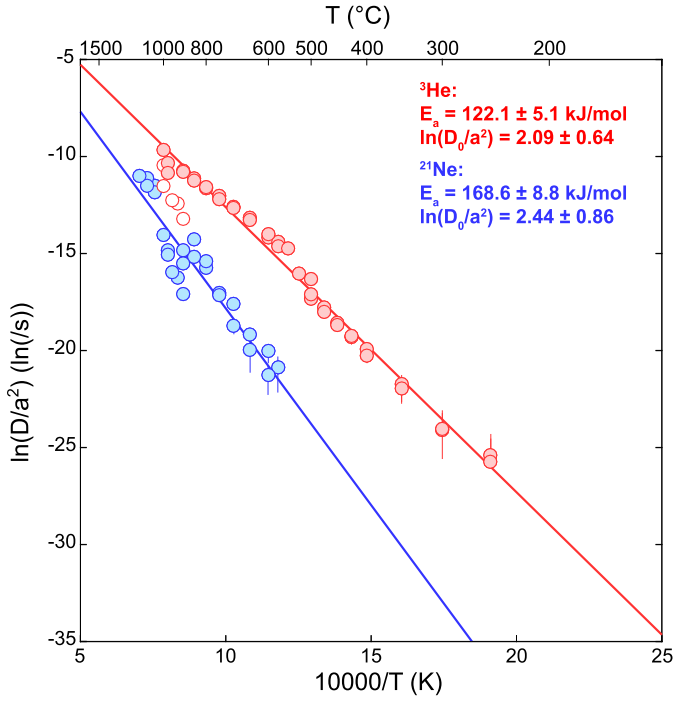

Fig. 4. An Arrhenius plot showing data collected in a bulk degassing experiment on a proton irradiated fragment of San Carlos olivine, and Arrhenius parameters inverted from the data. He and Ne data were collected simultaneously. We estimate an effective spherical radius of 330 μm for this grain (see Supplementary Fig. S4), yielding preexponentials of $8.80 \times 10^{-7+7.89\times10^{-7}}_{-4.16\times10-7}$ for He and $1.25 \times 10^{-6+1.70\times10^{-6}}_{-7.21\times10-7}$ for Ne.

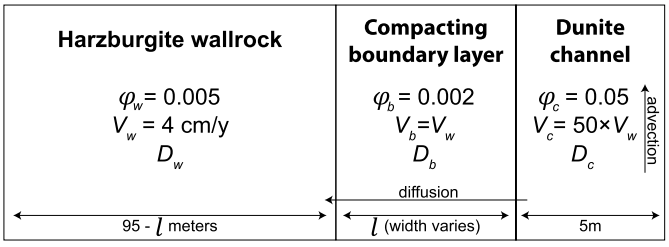

Fig. 5. Schematic illustrating our model setup. Vertical advection in the harzburgite wallrock and CBL is not shown as it provides a reference frame for our solutions. Total upwelling distance is 70 km. Diffusion in the vertical dimension is neglected.

reaches of dunite channels creates a compacting boundary layer (CBL) around channels with a very low melt fraction (Liang et al., 2010; Schiemenz et al., 2010), and melt–rock reaction at the dunite channel–wallrock interface consumes latent heat, producing a cold thermal boundary layer around the channel (e.g. Katz and Weatherly, 2012). In the models presented below, we test cases where the CBL is impermeable, and cases where it has low but finite permeability. We also explore how different CBL thicknesses affect the efficiency of fractionation of He from Ne in dunite channel wallrock.

3. A model for kinetic fractionation of He from Ne in the mantle

A schematic illustrating our model setup is shown in Fig. 5, which is similar to Kenyon (1990). The simulation domain is divided into three adjacent segments: harzburgite wallrock, a CBL with a relatively low melt fraction, and a dunite channel. The contact between the dunite channel and CBL is the origin in the horizontal (x) dimension. In all simulations the width of the simulation domain is 100 m, the dunite channel is 5 m wide; the width of the CBL varies as l. We assume melt upwells in the wallrock at a rate of 4 cm/y and use the wallrock-hosted melt as our reference frame. Melt in the dunite channel advects 50× faster than melt in the wallrock owing to its higher permeability (e.g., Kelemen et al., 1997). There is no lateral advection of melt; diffusion in the vertical (z) dimension is neglected. The composition of material in the dunite channel is given by

$$\frac{\partial C_c}{\partial t} + V_c \frac{\partial C_c}{\partial z} = D_c \frac{\partial^2 C_c}{\partial x^2}, \tag{1}$$

where D_c is the effective diffusion rate in the channel and V_c is the velocity of the channel melt in the z direction. The composition of the CBL is given by

$$\frac{\partial C_b}{\partial t} = D_b \frac{\partial^2 C_b}{\partial x^2}, \tag{2}$$

where D_b is the effective diffusion rate in the boundary layer. The composition of the harzburgite wallrock is given by

$$\frac{\partial C_w}{\partial t} = D_w \frac{\partial^2 C_w}{\partial x^2}, \tag{3}$$

where D_w is the effective diffusion rate in the wallrock. Compositions at the channel–CBL interface and CBL–harzburgite wallrock interface and are fixed by equilibrium constants

$$C_b(x=0) = K_{cb} C_c(x=0), \tag{4}$$

$$C_w(x=-l) = K_{bw} C_b(x=-l), \tag{5}$$

where K_{cb} is the bulk channel-CBL partition coefficient, and K_{bw} is the bulk CBL–wallrock partition coefficient, which depend on the relative phase proportions across these contacts (*effectively the melt fractions, as we treat noble gases as perfectly incompatible in silicate minerals*). Effective diffusion coefficients are given by

$$D_i = \frac{\varphi_i}{\sqrt{2}} D_{melt} + (1-\varphi_i) D_{solid}, \tag{6}$$

where φ_i is the melt fraction and diffusion in melt is scaled to correct for the tortuous matrix topology. In a second series of simulations we test cases where the CBL is impermeable; in those simulations, D_b is fixed at olivine volume diffusion rates. In all simulations, diffusion coefficients are calculated assuming a constant temperature of 1300 °C.

The maximum upwelling distance assumed (70 km) is the minimum height of the melting column beneath mid-ocean ridges suggested by isotopic and trace element evidence for garnet stability at the base of the MORB source melting region (cf. Kelemen et al., 1997, and references therein). This establishes the total time for upwelling of the wallrock melt (1.75 Myr). Initial concentrations of ^{3}He and ^{22}Ne in the wallrock are assumed to be 0, consistent with a few percent of near-fractional melting of the mantle before formation of dunite channel networks, and the very low partition coefficients of noble gases in mantle minerals ($\sim 10^{-4}$, Heber et al., 2007; Jackson et al., 2013a). The initial ^{3}He/^{22}Ne in the channel is 1.5; for the purpose of studying the kinetic fractionation process concentrations are arbitrary but assumed to be 0.075 ppm for ^{3}He, and 0.05 ppm for ^{22}Ne in the channel (bulk). Equations (1), (2) and (3) are solved numerically using a Crank–Nicholson finite difference method. The solver was tested against the exact solution to a constant surface diffusion problem (Supplementary Fig. S3) and found to be in excellent agreement.

4. Results

Diffusion profiles produced in representative simulations testing different He and Ne diffusivities are shown in Fig. 6 for a series of

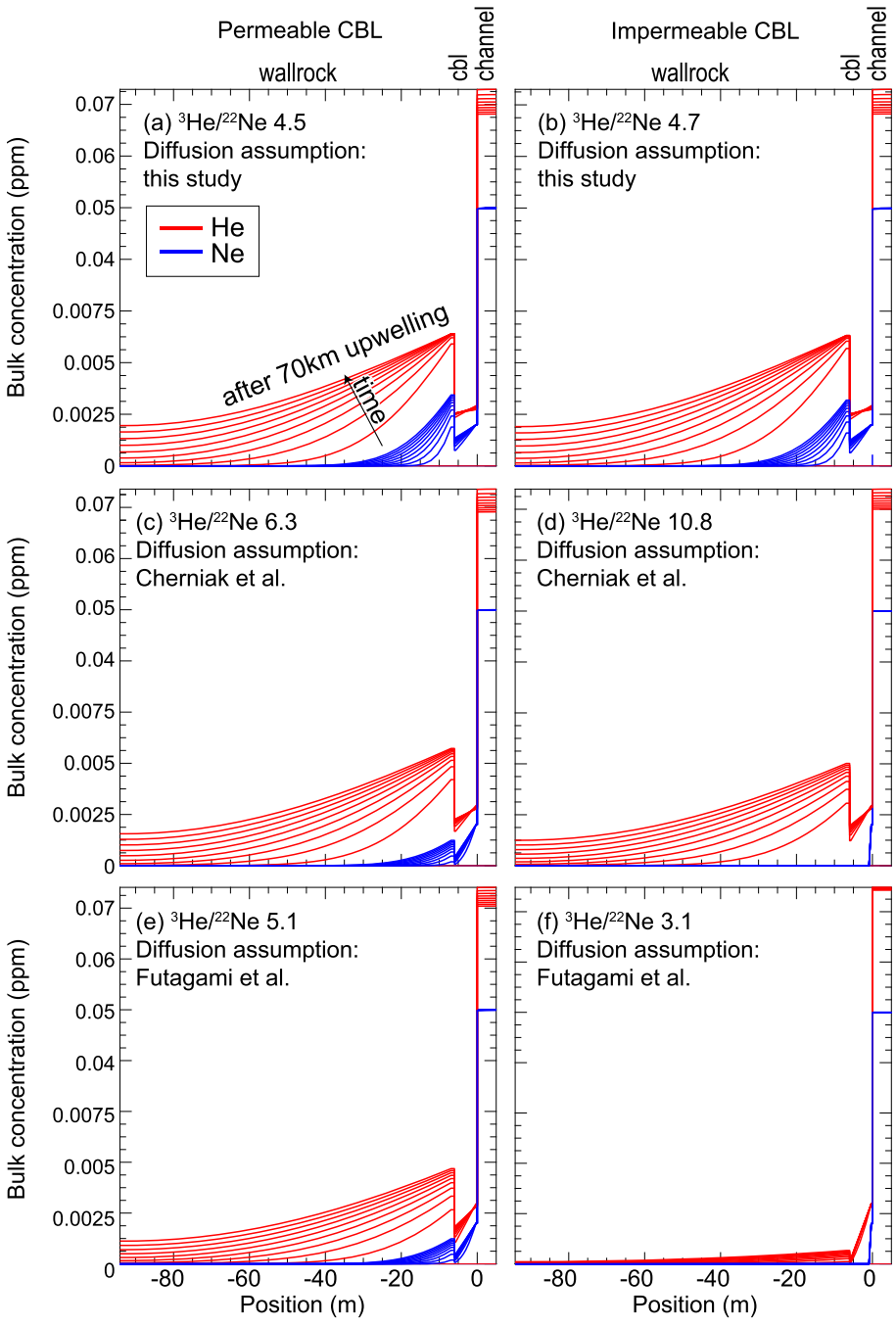

Fig. 6. Representative results from simulations assuming different diffusion coefficients and a 6 m thick compacting boundary layer. ^{3}He/^{22}Ne is the ratio of the regassed lithosphere after compaction of trapped melt to a residual value of 0.2% (see Section 4).

time steps; simulation assumptions are detailed in the figure caption. In general, ^{3}He concentrations decrease in the dunite-hosted melt as they increase in the wallrock; ^{22}Ne concentrations increase in the wallrock (and decrease in the channel) much more slowly. The simulations suggest that kinetic fractionation may efficiently modulate the ^{3}He/^{22}Ne of the depleted mantle within diffusive length scales around dunite channels beneath mid-ocean ridges. We emphasize that heavier noble gases will not be fractionated from one another by melt migration because of their slower diffusivities.

Dunite channels are thought to form a repeating network of dunite–wallrock units in triangular melting regions beneath mid-ocean ridges (Fig. 2a; also see Supplementary Fig. S4). Material in the melt triangle ultimately becomes lithosphere as it cools and advects away from the ridge axis due to corner flow. To estimate He and Ne concentrations and the average ^{3}He/^{22}Ne of the depleted mantle lithosphere, we input our simulation results into a melt triangle model assuming a 45–45–90 geometry and triangle depth of 70 km directly beneath the ridge axis. Asthenospheric mantle forms new lithosphere that advects laterally away from the ridge axis as it crosses the solidus owing to conductive cooling. The upwelling rate is assumed to be uniform across the base of the triangle; melting columns near the corners of the triangle experience less upwelling than columns near the center because they are cooled and rotated into the direction of seafloor spreading at greater depths. When a parcel of mantle reaches the lithosphere–asthenosphere boundary, it “freezes in” some fraction of trapped melt; here we assume 0.2% melt is frozen in the dunite, CBL and

wallrock (e.g., Sundberg et al., 2010). Depending on the choice of diffusion coefficients, CBL thickness, and diffusive pathway (i.e., permeable vs. impermeable CBL), our models produce a regassed mantle lithosphere with a $^3He/^{22}Ne$ ratio ~2–6× greater than the initial source value (Fig. 7a) and noble gas concentrations ~2–3 orders of magnitude below initial source values (Fig. 7b; c).

Oceanic lithosphere eventually passes through subduction zones where it can form a high $^3He/^{22}Ne$ MORB source, provided high $^3He/^{22}Ne$ mantle lithosphere is not fully degassed after subduction. The mantle's *heavy* noble gas (Ar–Xe) budget appears to be dominated by a recycled atmospheric component likely related to subduction of hydrothermally altered slab (e.g., Holland and Ballentine, 2006; Parai and Mukhopadhyay, 2015; Smye et al., 2017), but recycling of an atmospheric *light* noble gas (He–Ne) component has not had a demonstrable impact on mantle budgets. Because atmospheric $^3He/^{22}Ne$ in sediment and altered basalt is ~0, if surface-influenced portions of subducting slabs did not lose atmospheric Ne and He in subduction zones, the MORB source would have a lower $^3He/^{22}Ne$ than primordial sources (e.g., Tucker and Mukhopadhyay, 2014). Shallow regions of subducting lithosphere presumably lose noble gases and other volatiles from pore fluids (Sumino et al., 2010) and hydrous phases (Jackson et al., 2013b; Kendrick et al., 2011, 2018) owing to cracking, heating and prograde metamorphism (e.g., Chavrit et al., 2016; Holland and Ballentine, 2006; Staudacher and Allègre, 1988; Smye et al., 2017). Isotopic, lithologic, and geospeedometric evidence suggests hydration beneath oceanic spreading centers is limited to approximately the upper km of the mantle section (Dygert and Liang, 2015; Dygert et al., 2017; Gregory and Taylor, 1981; Rospabé et al., 2017). Seismic reflection–refraction data suggest hydration of old lithospheric slabs is restricted to the upper 10 km of mantle lithosphere (e.g., Han et al., 2016; Van Avendonk et al., 2011). Thus, it is reasonable to expect that most mantle lithosphere that passes through subduction zones is not hydrated, and that mantle-derived noble gases in thick lithospheric slabs pass through subduction zones, allowing them to impart their high $^3He/^{22}Ne$ signature on the convecting mantle.

5. A MORB mantle mixing model

Regassed mantle has He concentrations ~2–3 orders of magnitude lower than undegassed mantle that did not experience partial melting and kinetic fractionation beneath mid-ocean ridges (Figs. 7b, c). Thus, equal mixtures of undegassed and diffusively regassed mantle will have $^3He/^{22}Ne$ similar to undegassed mantle. In order to form a MORB source with high $^3He/^{22}Ne$, most of the MORB mantle must have cycled through the global mid-ocean ridge system at least once, and mantle mixing must be sufficiently slow to produce a large reservoir of unmixed, regassed mantle. Volumetrically smaller mixtures of regassed and undegassed mantle may form low $^3He/^{22}Ne$ component within the MORB source.

Here we adopt the methodology of Gonnermann and Mukhopadhyay (2009) (their analytical box model) to consider the formation of a high $^3He/^{22}Ne$ MORB source. This model differs from their numerical simulations in two fundamental ways: (1) we make no attempt to model the evolution of the OIB source, which we consider to have been partially isolated from the MORB source throughout geologic time (e.g., Caracausi et al., 2016; Mukhopadhyay, 2012; Mundl et al., 2017; Pető et al., 2013; Rizo et al., 2016), (2) we do not consider or advocate for a lower mantle that is isolated from the upper mantle. On the contrary, our results suggest that the MORB source has dominated the volume of the upper and lower mantle throughout geologic time (see Section 8).

Within the MORB source there are high and low $^3He/^{22}Ne$ reservoirs made up of components. The low $^3He/^{22}Ne$ reservoir is composed of "undegassed" component that experiences some mixing with subducted, high $^3He/^{22}Ne$ components; the high $^3He/^{22}Ne$ reservoir is composed of many "regassed" components

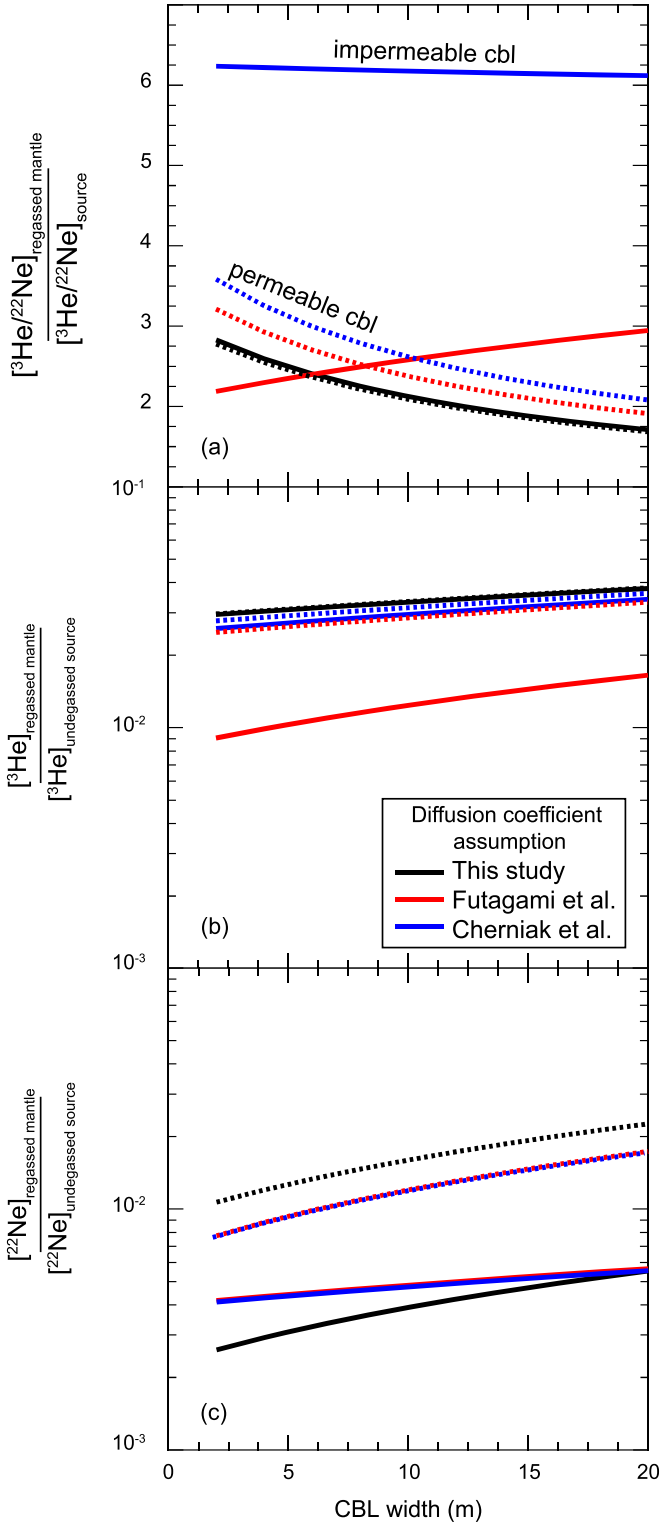

Fig. 7. $^3He/^{22}Ne$ regassed in mantle lithosphere relative to its initial source value from simulations assuming a permeable compacting boundary layer (solid lines) and an impermeable layer (dashed lines) as a function of compacting boundary layer thickness (a). Average He (b) and Ne (c) concentrations in the mantle lithosphere relative to initial mantle source concentrations. The extent of depletion of the regassed mantle relative to its undegassed mantle source is estimated assuming a 10% extent of melting.

that are partially consumed by mixing with low $^3He/^{22}Ne$ component,

$$\frac{M_d}{M_0} = \frac{N}{t}\int_0^t e^{(s-t)/\tau} ds. \quad (7)$$

M_d is the mass of depleted, high $^3He/^{22}Ne$ component produced at time s remaining in the MORB source at time t, M_0 is the initial mass of the MORB source, N is the number of MORB source masses processed through the global mid-ocean ridge system over time t, and τ is a characteristic mantle mixing timescale. Integrating,

$$\frac{M_d}{M_0} = 1 - \frac{N}{t}\tau - \frac{N}{t}\tau e^{-t/\tau}. \quad (8)$$

This model assumes that the MORB source was initially composed of a single body of primordial, low $^3He/^{22}Ne$ (~1.5) material that is consumed as high $^3He/^{22}Ne$ components are produced to form the high $^3He/^{22}Ne$ reservoir. The low $^3He/^{22}Ne$ reservoir in the MORB source melts preferentially because it is more fusible than the depleted, high $^3He/^{22}Ne$ reservoir (Fig. 8a).

Because He and Ne concentrations in regassed, high $^3He/^{22}Ne$ mantle are low, mixing between low and high $^3He/^{22}Ne$ components enlarges the low $^3He/^{22}Ne$ reservoir and shrinks the high $^3He/^{22}Ne$ reservoir. For a given N, a long τ produces a relatively large high $^3He/^{22}Ne$ reservoir; a short τ produces a relatively large low $^3He/^{22}Ne$ reservoir. Tradeoffs between characteristic mantle mixing timescales (τ) and the number of mantle masses fluxed through the global mid-ocean ridge system (N) are shown in Fig. 8b for cases where the MORB source is composed of $90 \pm 10\%$ high $^3He/^{22}Ne$ reservoir. This large extent of degassing can be accounted for by 4–9 MORB source masses being cycled through the global mid-ocean ridge system (e.g., Coltice et al., 2009; Tolstikhin et al., 2014), which corresponds to a τ value range of ~0.4–1 Gyr (Fig. 8b). Smaller N values require longer characteristic mantle mixing timescales. MORB mantle mixing timescales have been constrained using pseudochrons within the Rb–Sr, Sm–Nd, and U–Pb isotopic systems (Donnelly et al., 2004); mantle mixing timescales derived from these pseudochrons are roughly consistent with τ values explored here (~0.3 Gyr vs. ~0.4–1 Gyr). In scenarios where MORB source mixing timescales are shorter, volatile extraction by volcanism is inefficient because volatile-poor components within the MORB source are homogenized with and dominated by more volatile-rich components (Fig. 8; Gonnermann and Mukhopadhyay, 2009). Thus, the long MORB source mixing timescales suggested by the $^3He/^{22}Ne$ system are corroborated by observed depletion of radiogenic Xe isotopes and ^3He relative to radiogenically produced ^4He in the MORB source (see below, e.g., Class and Goldstein, 2005; Coltice et al., 2009; Davies, 2011; Parai and Mukhopadhyay, 2015; Porcelli and Elliott, 2008; Tolstikhin et al., 2014; Tucker et al., 2012).

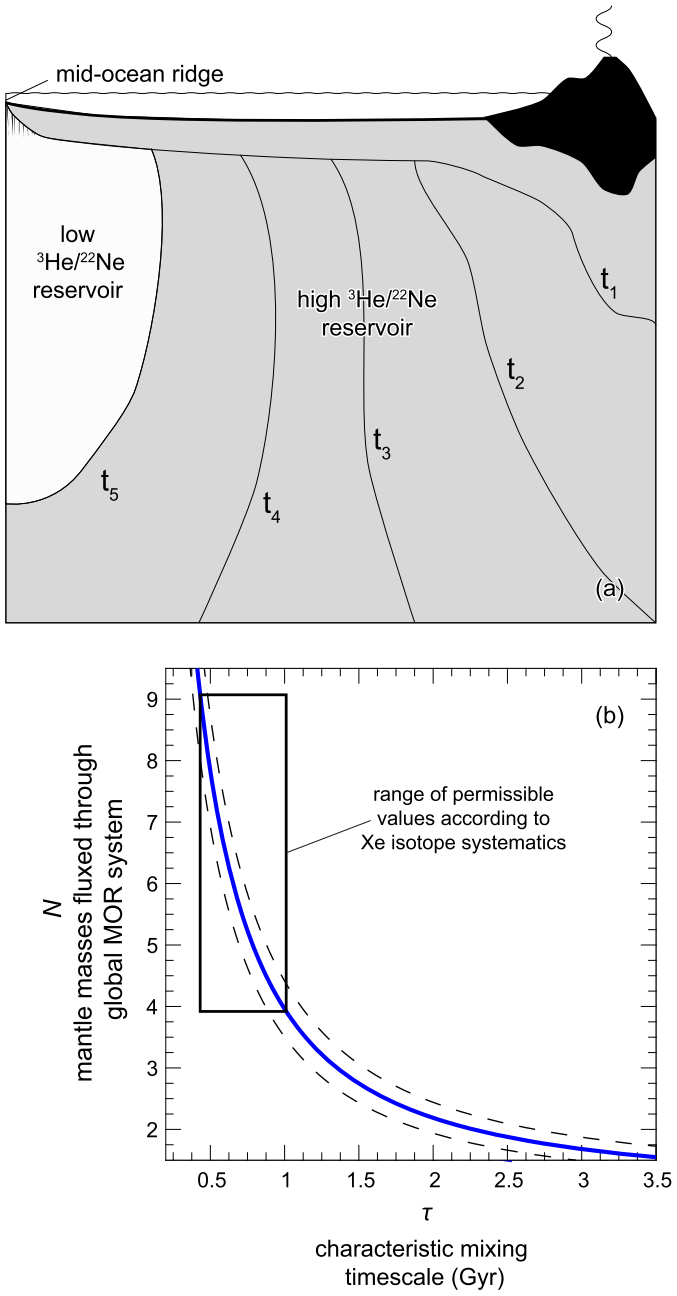

Fig. 8. (a) Cartoon illustrating the formation of a high $^3He/^{22}Ne$ MORB source according to the model of Gonnermann and Mukhopadhyay, 2009 (Eqs. (7) and (8)). The high $^3He/^{22}Ne$ reservoir, composed of many high $^3He/^{22}Ne$ components formed at different times, is produced by partial melting and kinetic fractionation of material originating from a primordial, low $^3He/^{22}Ne$ reservoir. Mixing between the low and high $^3He/^{22}Ne$ reservoirs shrinks the high $^3He/^{22}Ne$ reservoir and enlarges the low $^3He/^{22}Ne$ reservoir. If mixing is sufficiently slow, the high $^3He/^{22}Ne$ reservoir grows through time, as is shown here. (b) Tradeoff between the number of MORB source masses fluxed through the global mid-ocean ridge system (N) and the characteristic mantle mixing timescale (τ) needed to produce a MORB source composed of 90% of regassed, high $^3He/^{22}Ne$ mantle (solid line) according to Eq. (8). Dashed lines show cases with a MORB source composed of 10% more or less high $^3He/^{22}Ne$ mantle. The black box shows the range of permissible values according to Xe isotope systematics (e.g., Coltice et al., 2009; Tolstikhin et al., 2014).

6. Consistency of our model with other noble gas systems and mantle dynamics

6.1. Constraints on MORB source degassing from long-lived Xe and $^3He/^4He$ systematics

For regassed, high $^3He/^{22}Ne$ mantle to be a significant reservoir within the MORB source, degassing of primordial volatiles from the MORB mantle must have been extensive (>96%) owing to the low overall gas contents of regassed mantle. Evidence for extensive degassing of primordial volatiles comes from recent studies that demonstrate the MORB mantle contains very little Pu-derived Xe compared to U-derived Xe. Because Pu-derived Xe was produced before U-derived Xe, this observation implies >99% degassing of the MORB source primordial volatile budget throughout geologic time (e.g., Tolstikhin et al., 2014; Tucker et al., 2012; Parai and Mukhopadhyay, 2015). Similar extents (>99%) of degassing are implied by estimates of initial mantle ^3He concentration and present-

day MORB source $^{3}He/^{4}He$ systematics (e.g., Class and Goldstein, 2005; Porcelli and Elliott, 2008). Depending upon the isotopic system, estimates of timescales for achieving 99% MORB source degassing range from ~1.5 Gyr to all of geologic time (e.g., Tolstikhin et al., 2014 and references therein). The Xe system suggests extensive early degassing followed by a longer period of more measured degassing. Extensive early degassing could have been produced by vigorous Hadean volcanism, potentially superimposed on degassing associated with a Moon-forming giant impact. However, provided that He was fractionated from Ne around dunite channels for most of geologic time, no impact-related degassing is required by our model.

6.2. Consistency of extensive MORB source degassing with dynamic models and Earth's ^{40}Ar budget

Canonical estimates of Earth's ^{40}Ar budget place ~50% of all ^{40}Ar atoms in the mantle (Hart et al., 1985; Allègre et al., 1996). Because ^{40}Ar is strictly produced by the decay of ^{40}K and ^{40}K has a 1.25 Gyr half-life, this implies >50% degassing of the mantle's primordial volatile component. Within a purely whole mantle convection model framework, 50% degassing of ^{40}Ar is achieved in dynamic models at ~60% to 93% primordial element degassing, depending on Earth's thermal history (Brandenburg et al., 2008; Phipps-Morgan, 1998; van Keken and Ballentine, 1999). This range of primordial element degassing is less than the >96% required by the $^{3}He/^{22}Ne$ system within our model and the $^{3}He/^{4}He$ and Xe isotope systems. Within the dynamic models, higher MORB source primordial volatile degassing extents would be associated with 50% retention of ^{40}Ar if depth of melting scaled with mantle potential temperature and/or if a portion of the mantle ^{40}Ar budget were contained in a region separate from the MORB source (e.g., Ballmer et al., 2017; Kellogg et al., 1999; Mukhopadhyay, 2012; Tolstikhin et al., 2006). Unambiguous evidence for mantle reservoirs isolated from the MORB source throughout geologic time is given by the isotopic systematics of OIBs (Caracausi et al., 2016; Mukhopadhyay, 2012; Mundl et al., 2017; Pető et al., 2013; Rizo et al., 2016), providing at least one "hidden reservoir" to balance Earth's ^{40}Ar budget. However, we note that uncertainties in the mantle ^{40}K budget are significant, potentially eliminating any need to host ^{40}Ar in hidden mantle reservoirs (e.g., Lassiter, 2004). Thus, the requirement for large extents of MORB source primordial volatile degassing is consistent with the ^{40}Ar distribution in the Earth.

6.3. MORB source $^{3}He/^{4}He$ and $^{4}He/^{40}Ar$

The processes that cause kinetic fractionation of He from Ne around dunite channels in the MORB source will also fractionate He from U and Th. U and Th decay to produce ^{4}He; MORB melts and subcontinental lithospheric mantle have $^{3}He/^{4}He$ of $\lesssim 8R_A$ (R_A being the atmospheric ratio), far below the closed system value for a primitive mantle and suggesting long term depletion of ^{3}He relative to U + Th in the MORB source (e.g., Allègre et al., 1983; Day et al., 2005). Because U and Th diffusion rates are sluggish, our kinetic fractionation model would be expected to enrich the MORB mantle in ^{3}He relative to U + Th during melt migration beneath mid-ocean ridges, in apparent contradiction with a low $^{3}He/^{4}He$ MORB source. However, we invoke long-term subduction of oceanic crust along with high $^{3}He/^{22}Ne$ mantle lithosphere to form a high $^{3}He/^{22}Ne$ MORB source. Because U and Th are highly incompatible during mantle melting and the overwhelming majority of magmatic He is degassed, subducted lithosphere has a strongly elevated (U + Th)/He ratio. We modeled the evolution of $^{3}He/^{4}He$ in the depleted mantle assuming a fraction of U + Th in the subducted oceanic crust is mixed back into the high $^{3}He/^{22}Ne$ MORB source (Supplementary Figs. S5a; d). Our models suggest the regassed high $^{3}He/^{22}Ne$ mantle quickly recovers the signature low $^{3}He/^{4}He$ ratio associated with the MORB source by production of ^{4}He (Supplementary Fig. S5).

The $^{4}He/^{40}Ar$ ratio of the mantle is similar to or greater than values calculated assuming closed system accumulation of ^{4}He and ^{40}Ar due to the decay of U + Th and ^{40}K (e.g., Burnard, 2004; Honda and Patterson, 1999). Like He, U and Th, He may be expected to be fractionated from Ar around dunite channels owing to relatively sluggish diffusion of Ar in mantle materials, creating a high $^{4}He/^{40}Ar$ ratio regassed mantle that is inconsistent with some observations. However, the production rate of ^{4}He and ^{40}Ar (by U + Th and ^{40}K decay) is sufficiently fast such that the elevated $^{4}He/^{40}Ar$ of the regassed mantle is overwhelmed by decay of U + Th + K in the crustal component of the subducted slab. Models presented in Supplementary Figs. S5b; e suggest that after a fractionation event, the high $^{3}He/^{22}Ne$ MORB source quickly recovers $^{4}He/^{40}Ar$ values consistent with observations.

7. Evidence for kinetic fractionation of ^{3}He from ^{22}Ne

The most convincing verification of our kinetic fractionation model would come from direct observation of noble gas concentration gradients around dunite channels in ophiolites. We believe direct observation is unlikely because (1) serpentinization upon exhumation of mantle lithosphere may overprint preexisting noble gas signatures (Kendrick et al., 2011, 2018; Sumino et al., 2010), and (2) subsolidus reequilibration should be rapid enough to homogenize diffusion profiles over timescales relevant to lithospheric cooling.

Evidence for kinetic fractionation may alternatively be observed in basalts and mantle xenoliths. Near-fractional partial melting of the mantle, concomitant with transport-produced kinetic fractionation, will form mantle sources depleted in incompatible trace elements (e.g., Johnson et al., 1990; Sobolev and Shimizu, 1993) with elevated $^{3}He/^{22}Ne$. Parent isotopes are fractionated from daughter isotopes by mantle melting events, such that ancient, long-term depletion is recorded by radiogenic isotope ratios in abyssal peridotites unaffected by significant overprinting from melt impregnation (e.g., Mallick et al., 2014; Warren et al., 2009). Thus, we expect a correlation between $^{3}He/^{22}Ne$ and indices of long-term depletion such as radiogenic isotopes and incompatible trace element ratios. These correlations are observed within ^{87}Rb–^{87}Sr and ^{147}Sm–^{143}Nd isotope systems, and in La/Sm ratios in MORBs from around the world (Fig. 9; also see Tucker and Mukhopadhyay, 2014).

Whether these trends represent mixtures of basalts from more and less depleted sources or simply variations in the extent of source depletion is uncertain. Preservation of La/Nd–$^{3}He/^{22}Ne$ and radiogenic isotope-$^{3}He/^{22}Ne$ correlations requires that basalts subducted along with high $^{3}He/^{22}Ne$ mantle lithosphere lose some of their enrichment before being mixed back into the MORB source (e.g., Gonnermann and Mukhopadhyay, 2009), likely to continental crust, or that basaltic crust is partly decoupled from mantle lithosphere during subduction. If unmodified lithosphere were subducted back into MORB mantle, then MORB mantle would not be net depleted and the correlations shown in Fig. 9 would not be preserved.

Mantle peridotite xenoliths are often residues of partial melting and unaltered specimens can be obtained for analysis. They may faithfully record kinetic fractionation of ^{3}He from ^{22}Ne (or the lack thereof) depending on their melting history. Available data on the noble gas abundances in peridotite xenoliths are limited, but exhibit $^{3}He/^{22}Ne$ systematics consistent with trends among basalts. Hotspot-sourced xenoliths (Fig. 1d) have relatively low $^{3}He/^{22}Ne$, slightly elevated relative to their basaltic counterparts, as would be

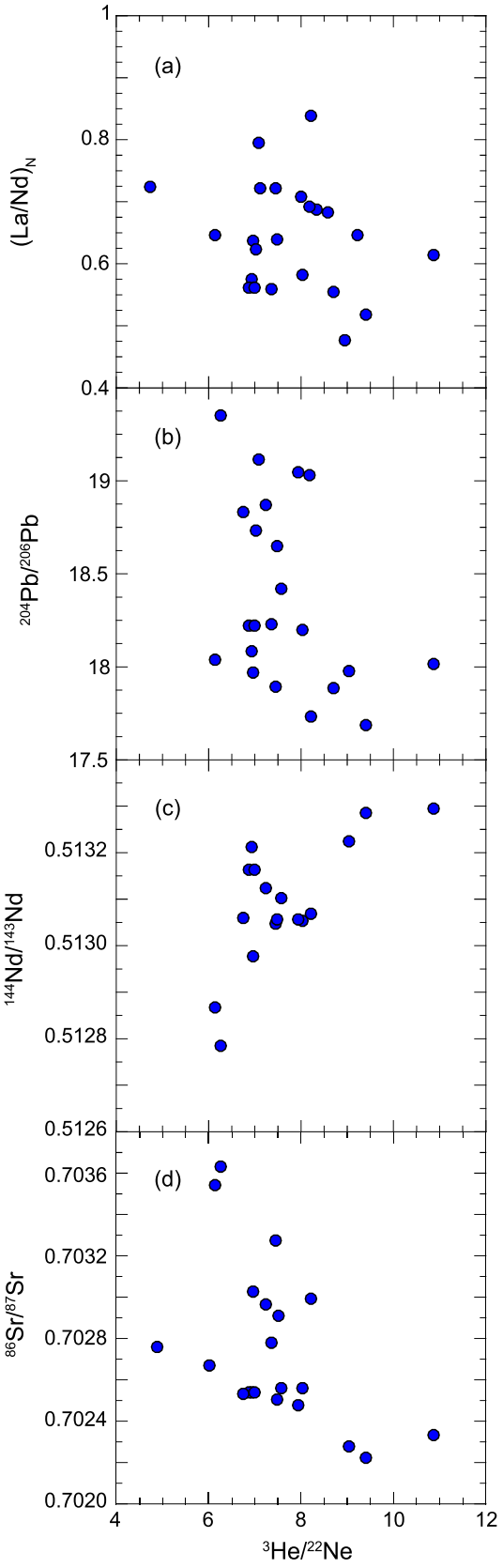

Fig. 9. Variations among $^{3}He/^{22}Ne$ and several indices of depletion; chondrite normalized La/Nd (a); $^{204}Pb/^{206}Pb$ (b); $^{144}Nd/^{143}Nd$ (c); $^{86}Sr/^{87}Sr$ (d). La/Nd, $^{144}Nd/^{143}Nd$, and $^{86}Sr/^{87}Sr$ show good correlations between $^{3}He/^{22}Ne$ and extent of source depletion, consistent with our model which predicts that samples with the highest $^{3}He/^{22}Ne$ should be the most depleted. Data used to prepare this figure are presented in the electronic repository; references are listed in the Electronic Supplement.

expected in a kinetic fractionation scenario. Subcontinental samples have greater variations in $^{3}He/^{22}Ne$ (Fig. 1e). Central European subcontinental lithospheric mantle (SCLM) is relatively low in $^{3}He/^{22}Ne$ and may be affected by a mantle plume (Buikin et al., 2005), but xenoliths from the Patagonian backarc have high and variable $^{3}He/^{22}Ne$ (Jalowitzki et al., 2016). Peridotites from arc environments that experienced high extents of partial melting are expected to have high $^{3}He/^{22}Ne$ ratios owing to repeated or prolonged kinetic fractionation events, consistent with the Patagonian xenoliths. However, because $^{3}He/^{22}Ne$ in SCLM xenoliths may be overprinted by interaction with metasomatic fluids/magmas, it is not clear which volatile sources are represented in SCLM xenolith compositions. The picture is further muddied by estimates of SCLM $^{3}He/^{22}Ne$ from well gas data which suggest ratios of 0.1–1.9 (Ballentine, 1997). However, these well gases are from crustal reservoirs with small mantle-derived components. Our model predicts a secular increase in the average MORB source $^{3}He/^{22}Ne$ throughout geologic time. Thus, we may anticipate that ancient SCLM has a $^{3}He/^{22}Ne$ closer to Earth's primordial value than younger SCLM. We encourage additional efforts to characterize the systematics of SCLM $^{3}He/^{22}Ne$.

8. Implications

Because the MORB mantle has an elevated $^{3}He/^{22}Ne$, the entire MORB source must have experienced at least one melt extraction and kinetic fractionation event. According to our simulations, each event removes 96–99% of the He and 98–99.7 of the Ne from the mantle source (Fig. 7). Subsequent melt extraction events will further deplete the MORB source. Thus, our models imply the MORB mantle is at least 96% degassed with respect to its primordial He and 98% degassed with respect to its primordial Ne, in agreement with previous estimates based on $^{3}He/^{4}He$ and Xe isotopes (e.g., Class and Goldstein, 2005; Davies, 2011; Porcelli and Elliott, 2008; Tolstikhin et al., 2014; Tucker et al., 2012). The near complete extraction of He and Ne likely extends to the full suite of Earth's primordial volatiles, given their similar behavior upon mantle melting (Aubaud et al., 2005; Heber et al., 2007; Jackson et al., 2013a; Keppler et al., 2003). This suggests that the primordial volatile content of the convecting mantle has been essentially lost to Earth's surface and that the modern volatile content of the mantle is dominated by recycling processes.

Kinetic fractionation around dunite channels may modulate the ratio of any relatively fast and slow diffusing element pairs in the depleted mantle (e.g., H/C, He/C, H/N, He/(U + Th)). H/C is high in the most H_2O depleted basalts (Hirschmann and Dasgupta, 2009), consistent with kinetic fractionation of light H from relatively heavy C around dunite channels. However, any element that is reintroduced to the mantle by subduction will have a more complicated cycling history than $^{3}He/^{22}Ne$, i.e., kinetic fractionation of many element pairs may not be observable in the compositions of erupted basalts due to recycling and mixing.

Seismic tomography suggests subducted slabs pass through the mantle transition zone (e.g., Grand, 2002; Fukao and Obayashi, 2013; Kárason and van der Hilst, 2000), which must be balanced by complementary mass transport from the lower to upper mantle (e.g., Forte et al., 2010). The timing associated with the onset of mantle convection across the transition zone, however, is unclear (e.g., Allègre, 1997; Davies, 1995). Our model requires convection across the transition zone throughout geologic history so that the low $^{3}He/^{22}Ne$ ratios of undegassed lower mantle do not dominate the modern day convecting mantle. Because mixtures of undegassed and regassed mantle will have low $^{3}He/^{22}Ne$ ratios, the preservation and prevalence of the high $^{3}He/^{22}Ne$ MORB source suggests the regions of the lower mantle that participate in

MORB mantle magmatism have already passed through the global mid-ocean ridge system at least once, i.e., mantle convection is not and has not been layered about the transition zone for most of geologic history. To preserve the high $^{3}He/^{22}Ne$ MORB source, exchange of noble gases between low $^{3}He/^{22}Ne$, high $^{3}He/^{4}He$ reservoirs and the depleted mantle must be limited, as suggested by Xe and W isotope systematics (e.g., Caracausi et al., 2016; Mukhopadhyay, 2012; Mundl et al., 2017; Pető et al., 2013; Rizo et al., 2016). This does not preclude mass exchange of less volatile elements, or exchange of volatiles between subducted materials and the OIB and MORB sources (Parai and Mukhopadhyay, 2015). Lowest and highest $^{3}He/^{22}Ne$ MORB mantle components likely reside in the lower mantle, where high viscosities impede mechanical stirring. If mixing is relatively rapid in the upper mantle, mixing timescales for the $^{3}He/^{22}Ne$ system predominantly reflect rates of mass exchange between the upper and lower mantle.

Acknowledgements

This work was inspired by a project for Yan Liang's kinetics class at Brown University. We thank S. Grand and J. Lassiter for useful discussions, P. van Keken for helpful comments on an earlier version of this manuscript, and constructive reviews by E.B. Watson and two anonymous reviewers. We acknowledge support from postdoctoral fellowships to N.D. by the Jackson School of Geosciences and C.J. by the Carnegie Institution for Science. M.M.T. was supported by a National Science Foundation Graduate Research Fellowship. D.L.S. and M.M.T. acknowledge support from the Anne and Gordon Getty Foundation.

Appendix A. Supplementary material

Supplementary material related to this article can be found online at https://doi.org/10.1016/j.epsl.2018.06.044.

References

Albarède, F., 2008. Rogue mantle helium and neon. Science 319, 943–945. https://doi.org/10.1126/science.1150060.

Allègre, C.J., 1997. Limitation on the mass exchange between the upper and lower mantle: the evolving convection regime of the Earth. Earth Planet. Sci. Lett. 150, 1–6.

Allègre, C.J., Hofmann, A., O'Nions, K., 1996. The Argon constraints on mantle structure. Geophys. Res. Lett. 23 (24), 3555–3557.

Allègre, C.J., Staudacher, T., Sarda, P., Kurz, M., 1983. Constraints on evolution of Earth's mantle from rare gas systematics. Nature 303, 762–766.

Amalberti, J., Burnard, P., Tissandier, L., Laporte, D., 2018. The diffusion coefficients of noble gases (He–Ar) in a synthetic basaltic liquid: one-dimensional diffusion experiments. Chem. Geol. 480, 35–43.

Aubaud, C., Hauri, E.H., Hirschmann, M.M., 2005. Hydrogen partition coefficients between nominally anhydrous minerals and basaltic melts. Geophys. Res. Lett. 31. https://doi.org/10.1029/2004GL021341.

Ballentine, C.J., 1997. Resolving the mantle He/Ne and crustal $^{21}Ne/^{22}Ne$ in well gases. Earth Planet. Sci. Lett. 152, 233–249.

Ballmer, M.D., Houser, C., Hernlund, J.W., Wentzcovitch, R.M., Hirose, K., 2017. Persistence of strong silica-enriched domains in the Earth's lower mantle. Nat. Geosci. 10. https://doi.org/10.1038/NGEO2898.

Barfod, D.N., Ballentine, J., Halliday, A.N., Fitton, J.G., 1999. Noble gases in the Cameroon line and the He, Ne, and Ar isotopic compositions of high μ (HIMU) mantle. J. Geophys. Res. 104, 29509–29527. https://doi.org/10.1029/1999JB900280.

Baxter, E.F., 2010. Diffusion of noble gases in minerals. Rev. Mineral. Geochem. 72, 509–557. https://doi.org/10.2138/rmg_2010.72.11.

Behrens, H., 2010. Noble gas diffusion in silicate glasses and melts. Rev. Mineral. Geochem. 72, 227–267.

Blard, P.-H., Puchol, N., Farley, K.A., 2008. Constraints on the loss of matrix-sited helium during vacuum crushing of mafic phenocrysts. Geochim. Cosmochim. Acta 72, 3378–3803. https://doi.org/10.1016/j.gca.2008.05.044.

Brandenburg, J.P., Hauri, E.H., van Keken, P.E., Ballentine, C.J., 2008. A multiple-system study of the geochemical evolution of the mantle with force-balanced plates and thermochemical effects. Earth Planet. Sci. Lett. 276, 1–13.

Buikin, A., Trieloff, M., Hopp, J., Althaus, T., Korochantseva, E., Schwarz, W.H., Altherr, R., 2005. Noble gas isotopes suggest deep mantle plume source of late Cenozoic mafic alkaline volcanism in Europe. Earth Planet. Sci. Lett. 230, 143–162. https://doi.org/10.1016/j.epsl.2004.11.001.

Burnard, P.G., 2004. Diffusive fractionation of noble gases and helium isotopes during mantle melting. Earth Planet. Sci. Lett. 220, 287–295.

Burnard, P.G., Demouchy, S., Delon, R., Arnaud, N.O., Marrocchi, Y., Cordier, P., Addad, A., 2015. The role of grain boundaries in the storage and transport of noble gases in the mantle. Earth Planet. Sci. Lett. 430, 260–270.

Burnard, P., Graham, D., Farley, K., 2004. Fractionation of noble gases (He, Ar) during MORB mantle melting: a case study on the Southeast Indian Ridge. Earth Planet. Sci. Lett. 227, 457–472. https://doi.org/10.1016/j.epsl.2004.08.021.

Caracausi, A., Avice, G., Burnard, P.G., Füri, E., Marty, B., 2016. Chondritic xenon in the Earth's mantle. Nature 533, 82–85.

Chavrit, D., Burgess, R., Sumino, H., Teagle, D.A.H., Droop, G., Shimizu, A., Ballentine, C.J., 2016. The contribution of hydrothermally altered ocean crust to the mantle halogen and noble gas cycles. Geochim. Cosmochim. Acta 183, 106–124. https://doi.org/10.1016/j.gca.2016.03.014.

Cherniak, D.J., Thomas, J.B., Watson, E.B., 2014. Neon diffusion in olivine and quartz. Chem. Geol. 371, 68–82.

Cherniak, D.J., Watson, E.B., 2012. Diffusion of helium in olivine at 1 atm and 2.7 GPa. Geochim. Cosmochim. Acta 84, 269–279.

Class, C., Goldstein, S.L., 2005. Evolution of helium isotopes in the Earth's mantle. Nature 436, 1107–1112. https://doi.org/10.1038/nature03930.

Coltice, N., Marty, B., Yokochi, R., 2009. Xenon isotope constraints on the thermal evolution of the early Earth. Chem. Geol. 266 (1–2), 4–9.

Davies, G.F., 1995. Punctuated tectonic evolution of the Earth. Earth Planet. Sci. Lett. 136, 363–379.

Davies, G.F., 2011. Dynamical geochemistry of the mantle. Solid Earth 2, 159–189. https://doi.org/10.5194/se-2-159-2011.

Day, J.M.D., Hilton, D.R., Pearson, D.G., Macpherson, C.G., Kjarsgaard, B.A., Janney, P.E., 2005. Absence of a high time-integrated $^{3}He/(U+Th)$ source in the mantle beneath continents. Geology 33 (9), 733–736. https://doi.org/10.1130/G21625.1.

Delon, R., Demouchy, S., Marrocchi, Y., Bouhifd, M.A., Baru, F., Cordier, P., Addan, A., Burnard, P.G., 2018. Helium incorporation and diffusion in polycrystalline olivine. Chem. Geol. https://doi.org/10.1016/j.chemgeo.2018.04.013 (in press).

Donnelly, K.E., Goldstein, S.L., Langmuir, C.H., Spiegelman, M., 2004. Origin of enriched ocean ridge basalts and implications for mantle dynamics. Earth Planet. Sci. Lett. 226, 347–366. https://doi.org/10.1016/j.epsl.2004.07.019.

Dygert, N., Kelemen, P.B., Liang, Y., 2017. Spatial variations in cooling rate in the mantle section of the Samail ophiolite in Oman: implications for formation of lithosphere at mid-ocean ridges. Earth Planet. Sci. Lett. 465, 134–144. https://doi.org/10.1016/j.epsl.2017.02.038.

Dygert, N., Liang, Y., 2015. Temperatures and cooling rates recorded in REE in coexisting pyroxenes in ophiolitic and abyssal peridotites. Earth Planet. Sci. Lett. 420, 151–161. https://doi.org/10.1016/j.epsl.2015.02.042.

Dygert, N., Liang, Y., Kelemen, P.B., 2016. Formation of plagioclase lherzolite and associated dunite–harzburgite–lherzolite sequence by multiple episodes of melt percolation and melt–rock reaction: an example from Trinity ophiolite. J. Petrol. 57 (4), 815–838. https://doi.org/10.1093/petrology/egw018.

Fechtig, H., Kalbitzer, S., 1966. The diffusion of argon in potassium-bearing solids. In: Potassium Argon Dating, pp. 68–107.

Forte, A.M., Quéré, S., Moucha, R., Simmons, N.A., Grand, S.P., Mitrovica, J.S., Rowley, D.B., 2010. Joint seismic-geodynamic-mineral physical modeling of African geodynamics: a reconciliation of deep-mantle convection with surface geophysical constraints. Earth Planet. Sci. Lett. 295, 329–341.

Frank, R.C., Swets, D.E., Lee, R.W., 1961. Diffusion of neon isotopes in fused quartz. J. Chem. Phys. 35 (4), 1451–1459. https://doi.org/10.1063/1.1732065.

Frischat, G.H., Oel, H.J., 1965. Determination of the diffusion coefficient of helium in glass from the shrinkage of a bubble. Glastech. Ber. 38 (4), 156–166.

Fukao, Y., Obayashi, M., 2013. Subducted slabs stagnant above, penetrating through, and trapped below the 660 km discontinuity. J. Geophys. Res. 118 (11). https://doi.org/10.1002/2013JB010466.

Futagami, T., Ozima, M., Nagai, S., Aoki, Y., 1993. Experiments on thermal release of implanted noble gases from minerals and their implications for noble gases in lunar soil grains. Geochim. Cosmochim. Acta 57, 3177–3194.

Gonnermann, H.M., Mukhopadhyay, S., 2007. Non-equilibrium degassing and a primordial source for helium in ocean-island volcanism. Nature 449, 1037–1040. https://doi.org/10.1038/nature06240.

Gonnermann, H.M., Mukhopadhyay, S., 2009. Preserving noble gases in a convecting mantle. Nature 459, 560–563.

Gourbet, L., Shuster, D.L., Balco, G., Cassata, W.S., Renne, P.R., Rood, D., 2012. Neon diffusion kinetics in olivine, pyroxene and feldspar: retentivity of cosmogenic and nucleogenic neon. Geochim. Cosmochim. Acta 86, 21–36. https://doi.org/10.1016/j.gca.2012.03.002.

Graham, D.W., 2002. Noble gas isotope geochemistry of mid-ocean ridge and ocean island basalts: characterization of mantle source reservoirs. Rev. Mineral. Geochem. 47, 247–317.

Grand, S.P., 2002. Mantle shear-wave tomography and the fate of subducted slabs. Phil. Trans. R. Soc. Lond. 360, 2475–2491.

Gregory, R.T., Taylor, H.P., 1981. An oxygen isotope profile in a section of cretaceous oceanic crust, Samail ophiolite, Oman: evidence for $\delta^{18}O$ buffering of the oceans by deep (>5 km) seawater-hydrothermal circulation at mid-ocean ridges. J. Geophys. Res. 86 (B4), 2737–2755.

Han, S., Carbotte, S.M., Canales, J.P., Nedimović, M.r., Carton, H., Gibson, J.C., Horning, G.W., 2016. Seismic reflection imaging of the Juan de Fuca plate from ridge to trench: new constraints on the distribution of faulting and evolution of the crust prior to subduction. J. Geophys. Res. 121 (3), 1849–1872. https://doi.org/10.1002/2015JB012416.

Harper, C.L., Jacobsen, S.B., 1996. Noble gases and Earth's accretion. Science 273, 1814–1818.

Hart, S.R., 1993. Equilibration during mantle melting: a fractal tree model. Proc. Natl. Acad. Sci. USA 90 (24), 11914–11915.

Hart, R., Hogan, L., Dymond, J., 1985. The closed-system approximation for evolution of argon and helium in the mantle, crust and atmosphere. Chem. Geol. 52, 45–73.

Heber, V.S., Brooker, R.A., Kelley, S.P., Wood, B.J., 2007. Crystal–melt partitioning of noble gases (helium, neon, argon, krypton, and xenon) for olivine and clinopyroxene. Geochim. Cosmochim. Acta 71, 1041–1061.

Hilton, D.R., Fischer, T.P., Marty, B., 2002. Noble gases and volatile recycling at subduction zones. Rev. Mineral. Geochem. 47, 319–370.

Hirschmann, M.M., Dasgupta, R., 2009. The H/C ratios of Earth's near-surface and deep reservoirs, and consequences for deep Earth volatile cycles. Chem. Geol. 262, 4–16.

Hofmann, A.W., 1980. Diffusion in natural silicate melts: a critical review. Phys. Magmatic Proces., 385–417.

Hofmann, A.W., Hart, S.R., 1978. An assessment of local and regional isotopic equilibrium in the mantle. Earth Planet. Sci. Lett. 38 (1), 44–62. https://doi.org/10.1016/0012-821X(78)90125-5.

Holland, G., Ballentine, C.J., 2006. Seawater subduction controls the heavy noble gas composition of the mantle. Nature 441, 186–191. https://doi.org/10.1038/nature04761.

Honda, M., McDougall, I., 1998. Primordial helium and neon in the Earth – a speculation on early degassing. Geophys. Res. Lett. 25, 1951–1954.

Honda, A., Patterson, D.B., 1999. Systematic elemental fractionation of mantle-derived helium, neon and argon in mid-oceanic ridge glasses. Geochim. Cosmochim. Acta 63, 2863–2874. https://doi.org/10.1016/S0016-7307(99)00206-9.

Iacono-Marziano, G., Paonita, A., Rizzo, A., Scaillet, B., Gaillard, F., 2010. Chem. Geol. 279, 145–157. https://doi.org/10.1016/j.chemgeo.2010.10.017.

Jackson, C.R.M., Parman, S.W., Kelley, S.P., Cooper, R.F., 2013a. Constraints on light noble gas partitioning at the conditions of spinel-peridotite melting. Earth Planet. Sci. Lett. 384, 178–187.

Jackson, C.R.M., Parman, S.W., Kelley, S.P., Cooper, R.F., 2013b. Noble gas transport into the mantle facilitated by high solubility in amphibole. Nat. Geosci. 6, 562–565. https://doi.org/10.1038/NGEO1851.

Jalowitzki, T., Sumino, H., Conceicao, R.V., Orihashi, Y., Nagao, K., Bertotto, G.W., Balbinot, E., Schilling, M.E., Gervasoni, F., 2016. Noble gas composition of subcontinental lithospheric mantle: an extensively degassed reservoir beneath Southern Patagonia. Earth Planet. Sci. Lett. 450, 263–273. https://doi.org/10.1016/j.epsl.2016.06.034.

Johnson, K.T.M., Dick, H.J.B., Shimizu, N., 1990. Melting in the oceanic upper mantle: an ion microprobe study of diopsides in abyssal peridotites. J. Geophys. Res. 95 (B3), 2661–2678.

Kárason, H., van der Hilst, R.D., 2000. Constraints on mantle convection from seismic tomography. Geophys. Monogr. 121, 227–288.

Katz, R.F., Weatherly, S.M., 2012. Consequences of mantle heterogeneity for melt extraction at mid-ocean ridges. Earth Planet. Sci. Lett. 335, 226–237.

Kelemen, P.B., Dick, H.J.B., Quick, J.E., 1992. Formation of harzburgite by pervasive melt/rock reaction in the upper mantle. Nature 358, 635–641.

Kelemen, P.B., Hirth, G., Shimizu, N., Spiegelman, M., Dick, H.J.B., 1997. A review of melt migration processes in the adiabatically upwelling mantle beneath oceanic spreading ridges. Phil. Trans. R. Soc. Lond. 355, 283–318.

Kelemen, P.B., Shimizu, N., Salters, V.J.M., 1995. Extraction of mid-ocean-ridge basalt from the upwelling mantle by focused flow of melt in dunite channels. Nature 375, 747–753.

Kellogg, L.J., Hager, B.H., van der Hilst, R.D., 1999. Compositional stratification in the deep mantle. Science 238, 1881–1884. https://doi.org/10.1126/science.238.5409.1881.

Kendrick, M.A., Scambelluri, M., Hermann, J., Padrón-Navarta, J.A., 2018. Halogens and noble gases in serpentinites and secondary peridotites: implications for seawater subduction and the origin of mantle neon. Geochim. Cosmochim. Acta 235, 285–304. https://doi.org/10.1016/j.gca.2018.03.027.

Kendrick, M.A., Scambelluri, M., Honda, M., Phillips, D., 2011. High abundances of noble gas and chlorine delivered to the mantle by serpentinite subduction. Nat. Geosci. 4, 807–812. https://doi.org/10.1038/NGEO1270.

Kenyon, P.M., 1990. Trace element and isotopic effects arising from magma migration beneath mid-ocean ridges. Earth Planet. Sci. Lett. 101, 367–378.

Kenyon, P.M., 1993. Trace elements in migrating high-temperature fluids: effects of diffusive exchange with the adjoining solid. J. Geophys. Res. 98 (B12), 22007–22020. https://doi.org/10.1029/93JB02265.

Keppler, H., Wiedenbeck, M., Scheka, S.S., 2003. Carbon solubility in olivine and the mode of carbon storage in the Earth's mantle. Nature 424, 414–416. https://doi.org/10.1038/nature01828.

Lassiter, J.C., 2004. Role of recycled oceanic crust in the potassium and argon budget of the Earth: toward a resolution of the "missing argon" problem. Geochem. Geophys. Geosyst. 4 (11). https://doi.org/10.1029/2004GC000711.

Liang, Y., Schiemenz, A., Hesse, M.A., Parmentier, E.M., Hesthaven, J.S., 2010. High-porosity channels for melt migration in the mantle: top is the dunite and bottom is the harzburgite and lherzolite. Geophys. Res. Lett. 37, L15306.

Lux, G., 1987. The behavior of noble gases in silicate liquids: solution, diffusion, bubbles and surface effects, with applications to natural samples. Geochim. Cosmochim. Acta 51, 1549–1560.

Mahaffy, P.R., Donahue, T.M., Atreya, S.K., Owen, T.C., Niemann, H.B., 1998. Galileo probe measurements of D/H and $^3He/^4He$ in Jupiter's atmosphere. Space Sci. Rev. 84 (1), 251–263. https://doi.org/10.1023/A:1005091806594.

Mallick, S., Dick, H.J.B., Sachi-Kocher, A., Salters, V.J.M., 2014. Isotope and trace element insights into heterogeneity of subridge mantle. Geochem. Geophys. Geosyst. 15. https://doi.org/10.1002/2014GC005314.

Mukhopadhyay, S., 2012. Early differentiation and volatile accretion recorded in deep-mantle neon and xenon. Nature 486, 101–104.

Mulfinger, H.-O., Scholze, H., 1962. Solubility and diffusion of helium in glass melts: I. Glastech. Ber. 35 (11), 466–478.

Mundl, A., Touboul, M., Jackson, M.G., Day, J.M.D., Kurz, M.D., Lekic, V., Helz, R.T., Walker, R.J., 2017. Tungsten-182 heterogeneity in modern ocean island basalts. Science 356, 66–69.

Ott, U., 2002. Noble gases in meteorites-trapped components. Rev. Mineral. Geochem. 47, 71–100. https://doi.org/10.2138/rmg.2002.47.3.

Parai, R., Mukhopadhyay, S., 2015. The evolution of MORB and plume mantle volatile budgets: constraints from fission Xe isotopes in Southwest Indian Ridge basalts. Geochem. Geophys. Geosyst. 16. https://doi.org/10.1002/2014GC005566.

Pető, M.K., Mukhopadhyay, S., Kelley, K.A., 2013. Heterogeneities from the first 100 million years recorded in deep mantle noble gases from the Northern Lau Back-arc Basin. Earth Planet. Sci. Lett. 369–370, 13–23.

Phipps-Morgan, J.P., 1998. Thermal and rare gas evolution of the mantle. Chem. Geol. 145 (3–4), 431–445.

Porcelli, D., Elliott, T., 2008. The evolution of He isotopes in the convecting mantle and the preservation of high $^3He/^4He$ ratios. Earth Planet. Sci. Lett. 269, 175–185.

Rizo, H., Walker, R.J., Carlson, R.W., Horan, M.F., Mukhopadhyay, S., Manthos, V., Francis, D., Jackson, M.G., 2016. Preservation of Earth-forming events in the tungsten isotopic composition of modern flood basalts. Science 352, 809–812.

Rospabé, M., Ceuleneer, G., Benoit, M., Abily, B., Pinet, P., 2017. Origin of the dunitic mantle–crust transition zone in the Oman ophiolite: the interplay between percolating magmas and high-temperature hydrous fluids. Geology 45 (5), 471–474. https://doi.org/10.1130/G38778.1.

Schiemenz, A., Liang, Y., Parmentier, E.M., 2010. A high-order numerical study of reactive dissolution in an upwelling heterogeneous mantle, I: channelization, channel lithology and channel geometry. Geophys. J. Int. 186, 641–664.

Shuster, D.L., Farley, K.A., Sisterson, J.M., Burnett, D.S., 2004. Quantifying the diffusion kinetics and spatial distributions of radiogenic ^4He in minerals containing proton-induced ^3He. Earth Planet. Sci. Lett. 217, 19–32.

Smye, A.J., Jackson, C.R.M., Konrad-Schmolke, M., Hesse, M.A., Parman, S.W., Shuster, D.L., Ballentine, C.J., 2017. Noble gases recycled into the mantle through cold subduction zones. Earth Planet. Sci. Lett. 471, 65–73. https://doi.org/10.1016/j.epsl.2017/04.046.

Sobolev, A.V., Shimizu, N., 1993. Ultra-depleted primary melt included in an olivine from the Mid-Atlantic Ridge. Nature, 151–154.

Spiegelman, M., Kelemen, P.B., 2003. Extreme chemical variability as a consequence of channelized melt transport. Geochem. Geophys. Geosyst. 4. https://doi.org/10.1029/2002GC000336.

Spiegelman, M., Kelemen, P.B., Aharonov, E., 2001. Causes and consequences of flow organization during melt transport: the reaction infiltration instability in compactible media. J. Geophys. Res. 106 (B2), 2061–2077. https://doi.org/10.1029/2000JB900240.

Spiegelman, M., Kenyon, P., 1992. The requirements for chemical disequilibrium during magma migration. Earth Planet. Sci. Lett. 109 (3–4), 611–620. https://doi.org/10.1016/0012-821X(92)90119-G.

Staudacher, T., Allègre, C.J., 1988. Recycling of oceanic crust and sediments: the noble gas subduction barrier. Earth Planet. Sci. Lett. 89, 173–183.

Suhr, G., Hellebrand, E., Snow, J.E., Seck, H.A., Hofmann, A.W., 2003. Significance of large, refractory dunite bodies in the upper mantle of the Bay of Islands Ophiolite. Geochem. Geophys. Geosyst. 4. https://doi.org/10.1029/2001GC000277.

Sumino, H., Burgess, R., Mizukami, T., Wallis, S.R., Holland, G., Ballentine, C.J., 2010. Seawater-derived noble gases and halogens preserved in exhumed mantle wedge peridotite. Earth Planet. Sci. Lett. 294, 163–172. https://doi.org/10.1016/j.eps.2010.03.029.

Sundberg, M., Hirth, G., Kelemen, P.B., 2010. Trapped melt in the Josephine peridotite: implications for permeability and melt extraction in the upper mantle. J. Petrol. 51 (1–2), 185–200. https://doi.org/10.1093/petrology/egp089.

Swets, D.E., Lee, R.W., Frank, R.C., 1961. Diffusion coefficients of helium in fused quartz. J. Chem. Phys. 35 (17), 17–22. https://doi.org/10.1063/1.1731562.

Tolstikhin, I., Kamensky, I., Tarakanov, S., Kramers, J., Pekala, M., Skiba, V., Gannibal, M., Novikov, D., 2010. Noble gas isotope sites and mobility in mafic rocks and olivine. Geochim. Cosmochim. Acta 74, 1436–1447. https://doi.org/10.1016/j.gca.2009.11.001.

Tolstikhin, I.N., Kramers, J.D., Hofmann, A.W., 2006. A chemical Earth model with whole mantle convection: the importance of a core–mantle boundary layer (D″) and its early formation. Chem. Geol. 226, 79–99.

Tolstikhin, I., Marty, B., Porcelli, D., Hofmann, A., 2014. Evolution of volatile species in the Earth's mantle: a view from xenology. Geochim. Cosmochim. Acta 136, 229–246.

Trieloff, M., Kunz, J., 2005. Isotope systematics of noble gases in the Earth's mantle: possible sources of primordial isotopes and implications for mantle structure. Phys. Earth Planet. Inter. 148 (1), 13–38.

Tucker, J.M., Mukhopadhyay, S., 2014. Evidence for multiple magma ocean outgassing and atmospheric loss episodes from mantle noble gases. Earth Planet. Sci. Lett. 393, 254–256.

Tucker, J.M., Mukhopadhyay, S., Schilling, J.-G., 2012. The heavy noble gas composition of the depleted MORB mantle (DMM) and its implications for the preservation of heterogeneities in the mantle. Earth Planet. Sci. Lett. 355–356, 244–254. https://doi.org/10.1016/j.epsl.2012.08.025.

Van Avendonk, H.J.A., Holbrook, W.S., Lizarralde, D., Denyer, P., 2011. Structure and serpentinization of the subducting Cocos plate offshore Nicaragua and Costa Rica. Geochem. Geophys. Geosyst. https://doi.org/10.1029/2011GC003592.

van Keken, P.E., Ballentine, C.J., 1999. Dynamical models of mantle volatile evolution and the role of phase transitions and temperature-dependent rheology. J. Geophys. Res. 104 (B4), 7137–7151.

Wang, K., Brodholt, J., Lu, X., 2015. Helium diffusion in olivine based on first principles calculations. Geochim. Cosmochim. Acta 156, 145–153. https://doi.org/10.1016/j.gca.2015.01.023.

Warren, J.M., Shimizu, N., Sakaguchi, C., Dick, H.J.B., Nakamura, E., 2009. An assessment of upper mantle heterogeneity based on abyssal peridotite isotopic compositions. J. Geophys. Res. 114. https://doi.org/10.1029/2008JB006186.

Wendler, M., Kruner, H., Frischat, G.H., 1995. Gas bubbles in glass melts under microgravity, part 3: a further helium diffusion experiment. Phys. Chem. Glasses 36, 109–113.

Weston, B., Burgess, R., Ballentine, C.J., 2015. Disequilibrium degassing model determination of the ^{3}He concentration and ^{3}He/^{22}Ne of the MORB and OIB mantle sources. Earth Planet. Sci. Lett. 410, 128–139. https://doi.org/10.1016/j.epsl.2014.11.021.

Winchell, P., 1969. The compensation law for diffusion in silicates. High Temp. Sci. 1 (2), 200–215.

Yamamoto, J., Nishimura, K., Sugimoto, T., Takemura, K., Takahata, N., Sano, Y., 2009. Diffusive fractionation of noble gases in mantle with magma channels: origin of low He/Ar in mantle-derived rocks. Earth Planet. Sci. Lett. 280, 167–174. https://doi.org/10.1016/j.epsl.2009.01.029.